Supplementary Information (SI) for ChemComm.
This journal is © The Royal Society of Chemistry 2026

Electronic Supplementary Information

Bimetallic Metal-Organic Frameworks enable tandem catalysis for Efficient Electrocatalytic Nitrate Reduction and Zn-NO_3^- Batteries

*Long Lin, Tang Wang, Yu Zhou, Men Du, Rui Li, and Wang Zhang**

College of Materials Science and Engineering, College of Environment, State Key Laboratory of Advanced Separation Membrane Materials, Zhejiang Key Laboratory of Low-carbon Control Technology for Industrial Pollution, Zhejiang University of Technology, Hangzhou 310014, China.

E-mail: *zhangwang@zjut.edu.cn*

Materials

Copper nitrate hexahydrate ($Cu(NO_3)_2{\cdot}3H_2O$, >99.0%), Nickel nitrate hexahydrate ($Ni(NO_3)_2{\cdot}6H_2O$, >99.0%), Cobalt nitrate hexahydrate ($Co(NO_3)_2{\cdot}6H_2O$, >99.0%), Ferrous chloride tetrahydrate ($FeCl_2{\cdot}4H_2O$, >99.0%), polyvinylpyrrolidone (PVP, F.W. GR),N, N-dimethylformamide (DMF), Ethanol (EtOH), potassium hydroxide (KOH, 85%),hydrochloric acid (HCl, 12 mol/L), salicylic acid ($C_7H_6O_3$), trisodium citrate dihydrate($C_6H_5Na_3O_7{\cdot}2H_2O$) were purchased from Sinopharm Chemical Reagent Co. Ltd. 2.6-Naphthalene dicarboxylic acid ($C_{12}H_8O_4$(NDC), >99.0%), Sodiumhydroxide (NaOH), Phosphoric acid (>99.99%), sodium hypochlorite solution (NaClO, 0.1M)were purchased from Macklin Co. Ltd. Potassium nitrate (KNO_3, 99%), potassium nitrate-^{15}N($K^{15}NO_3$, 99%), ammonium chloride-^{15}N ($^{15}NH_4Cl$), sulfamic acid, sodium nitroferricyanidedihydrate ($C_5FeN_6Na_2O{\cdot}2H_2O$) were purchased from Aladdin Chemistry Co. Ltd. sulfoxide-d6(DMSO-d_6), Sulfanilamide, N-(1-Naphthyl) ethylenediamine dihydrochloride were purchased from damas beta Co. Ltd. Allexperiments were conducted using ultrapure water with a resistivity of 18.2 MΩ cm.

Synthesis of Cu-NDC

Take Cu-NDC for example, solution A was prepared by dissolving 0.204 g of $Cu(NO_3)_2{\cdot}3H_2O$ in 6 mL of deionized water. Solution B was obtained by dissolving 0.208 g of 2,6-Naphthalenedicarboxylic acid (NDC) in 24 mL of DMF. Meanwhile, 3.55 g of PVP was dissolved in 18 mL of deionized water under continuous stirring to form solution C. Subsequently, solution A was slowly poured into solution C and stirred for 10 min, followed by the addition of solution B and further stirring for 10 min. The resulting mixed solution was transferred into a Teflon-lined autoclave and heated at 100 ºC for 24 h. After cooling to room temperature, the precipitates were washed with ultrapure water and ethanol twice using a high-speed centrifuge at 8000 rpm for 5 min. Finally, the product was vacuum-dried overnight at 80 ºC to obtain the blue powder of Cu-NDC.

Synthesis of Cu/M-NDC

The synthesis steps of Cu/Fe-NDC, Cu/Co-NDC, and Cu/Ni-NDC are the same as those for Cu-NDC, except for the addition of corresponding metal salts in solution A. Specifically, to prepare Cu/Fe-NDC, 0.204 g of Cu(NO3)2·$3H_2O$ and 0.0252 g of $FeCl_2{\cdot}4H_2O$ were dissolved in 6 mL of deionized water to obtain solution A. Similarly, for Cu/Co-NDC and Cu/Ni-NDC, the additional metal precursors in solution A were replaced by 0.0369 g of $Co(NO3)_2{\cdot}6H_2O$ and 0.0368 g of $Ni(NO_3)_2{\cdot}6H_2O$, respectively.

Material characterizations

Scanning electron microscopy (SEM) measurements were performed using an FEI Nova-450 instrument with an electron beam voltage at 10 kV. energy dispersive X-ray spectroscopy (EDS) spectra and elemental mapping images were obtained by a FEI Talos S-FEG electron microscopy at 200 kV. Powder X-ray diffraction (XRD) patterns were obtained using a D/max-Ultima IV X-ray diffractometer. Raman spectra were collected using a Renishaw 2000 instrument. X-ray photoelectron spectroscopy (XPS) measurements were performed on a Thermo Scientific K- Alpha XPS instrument (Al K α source is 1486.6 eV).

NO_3RR tests

The NO_3RR electrochemical tests were all performed in H-type electrolytic cells consisting of an anode chamber and a cathode chamber separated by a Nafion 117 membrane. 1 M KOH solution (70 mL) with and without 32.3 mM NO_3^- (2000 ppm NO_3^- concentration) were uniformly distributed in the cathode and anode chambers, respectively. All electrochemical tests are performed in a standard three-electrode system, along with a graphite

rod and Hg/HgOelectrode as the reference electrode and counter electrode, respectively. The prepared working electrode should be activated by 300 cycles of the cyclic voltammetry (CV) at a scan rate of 100 mV s^{-1} to obtain stable curves. Linear sweep voltammetry (LSV) polarization curves were performed with a scan rate of 10 mV s^{-1}. The chronoamperometry (CA) was carried out at various potentials from -0.3 to -0.8 V vs. RHE for 20 min. All potentials were measured against the Hg/HgO reference electrode and converted to the RHE reference scale by E (vs. RHE) = E (vs. Hg/HgO) + 0.098 V + 0.0592 × pH.

Determination of NH_3 concentration

The indophenol blue method was utilized to colorimetrically analyze the generated NH_3. Initially, the post-reaction cathodic electrolyte was sampled and diluted to 2 mL. Then, the coloring agents were successively mixed into the diluted sample: 2 mL of a coloring reagent (1 M NaOH mixed with 5 wt.% salicylic acid and 5 wt.% sodium citrate), 1 mL of 0.05 M NaClO, and 0.2 mL of 1 wt.% sodium nitroferricyanide. After being stored in the dark for 2 h, the mixture's absorbance at 655 nm was evaluated via UV-vis spectrophotometry. The exact NH_3 amounts were calculated according to a standard calibration curve constructed using 0.0–5.0 μg/mL NH_4Cl standard solutions.

Determination of NO_3^- concentration

For NO_3^- quantification, a specific volume of the post-test electrolyte was initially diluted to 5 mL. Subsequently, 0.1 mL of 1 M HCl and 0.01 mL of 0.8 wt.% sulfamic acid were added to the dilution. Following a 30-min incubation in the dark, the sample was analyzed via UV-vis spectrophotometry. The final corrected absorbance was obtained using the formula: $A=A_{220nm}-2A_{275nm}$. The precise NO_3^- concentrations were then derived based on a standard calibration curve constructed from KNO_3^- reference solutions (0.0, 1.0, 2.0, 2.5, 5.0, 10.0, 15.0, and 20.0 μg/mL of NO_3^-.

Determination of NO_2^- concentration

The colorimetric reagent was prepared by dissolving 2 g of p-aminobenzenesulfonamide and 1 g of N-(1-naphthyl)ethylenediamine dihydrochloride sequentially into an acidic mixture (25 mL deionized H_2O and 5 mL phosphoric acid). For NO_2^- detection, a fraction of the tested electrolyte was diluted to 5 mL, followed by the addition of 0.1 mL of the aforementioned reagent. After a 20-min color-developing incubation, the absorbance of the mixture was measured at 540 nm via UV-vis spectrophotometry. The NO_2^- content was calibrated against a standard curve derived from 0.0–2.5 μg/mL $NaNO_2$ reference solutions.

^{15}N isotope-labeling experiment

To confirm the source of NH_3 qualitatively, electrochemical experiments were conducted using Cu/Fe-NDC catalyst on $^{14}NO_3^-$ + 1 M KOH and $^{15}NO_3^-$ (>98 atom%15N, ≥99% purity) + 1 M KOH electrolytes for 20 min electrolysis at -0.60 V (vs. RHE), respectively. The resulting solutions with and without electrolysis were respectively added with maleic acid and regulated to pH 1~2 using hydrochloric acid (4 M). Then, 0.5 mL of the solution was mixed thoroughly with 50 μL of DMSO-d6 for 1H NMR (400 MHz, Avance NEO) tests.To quantify the $^{14}NH_4^+$ yield after electrolysis of 32.3 mM NO_3^- (2000 ppm NO_3^- concentration) at -0.60 V (vs. RHE) for 20 min, a calibration curve from 1H NMR measurements was constructed using a series of $^{14}NH_4Cl$ solutions with defined concentrations (2.5, 50, 100 ,150 and 200 ppm) as standards. The peak area integral ratio of $^{14}NH_4^+$ to maleic acid was positively correlated with the concentrations of $^{14}NH_4^+$.

Calculation of the FE and Yield

The formation rates (mass-normalized yields) of the target product NH_3 and the primary byproduct NO_2^- were calculated according to the following formulas:

$$\text{Yield}_{NH_3} = \frac{C_{NH_3} \times V}{t \times m} \quad \text{(Equation 1)}$$

$$FE = \frac{8 \times F \times C_{NH_3} \times V}{M_{NH_3} \times Q} \quad \text{(Equation 2)}$$

To evaluate the selectivity of electron utilization during the electrocatalytic process, the Faradaic efficiencies FEs for ammonia and nitrite were determined using the equations below:

$$\text{Yield}_{NO_2^-} = \frac{C_{NO_2^-} \times V}{t \times m} \quad \text{(Equation 3)}$$

$$FE = \frac{2 \times F \times C_{NO_2^-} \times V}{M_{NO_2^-} \times Q} \quad \text{(Equation 4)}$$

Where C_{NH3} and C_{NO2-} denote the measured concentrations of ammonia and nitrite. V, t, and m represent the electrolyte volume (70 mL), electrolysis time (20 min), and catalyst loading mass (1 mg), respectively. M_{NH3} and M_{NO2-} are the corresponding molar masses. F is the Faraday constant (96485 C mol^{-1}), Q is the total charge (C), and 8 and 2 are the transferred electrons for forming NH_3 and NO_2^-, respectively.

Zn-NO_3^- battery performance

Carbon paper/nickel foam mixed substrate loaded with catalysts (1 mg cm^{-2}) and Zn foil (7× 2.5 × 0.2 cm^3) were used as the cathode and anode for the self-made zinc-nitrate battery, respectively. The battery that contains catholyte (1 M KOH+0.1 M KNO_3) and anolyte (6.0 M KOH+0.2 M $Zn(CH_3COO)_2$) separated by a proton exchange membrane (Nafion 117). All corresponding electrochemical measurements were processed with CHI 760. The battery- related evaluation parameters are calculated as follows:

The power density P: $P = I \times V$ (Equation 5)

where I is the dispatch current density; V is the dispatch voltage, respectively.

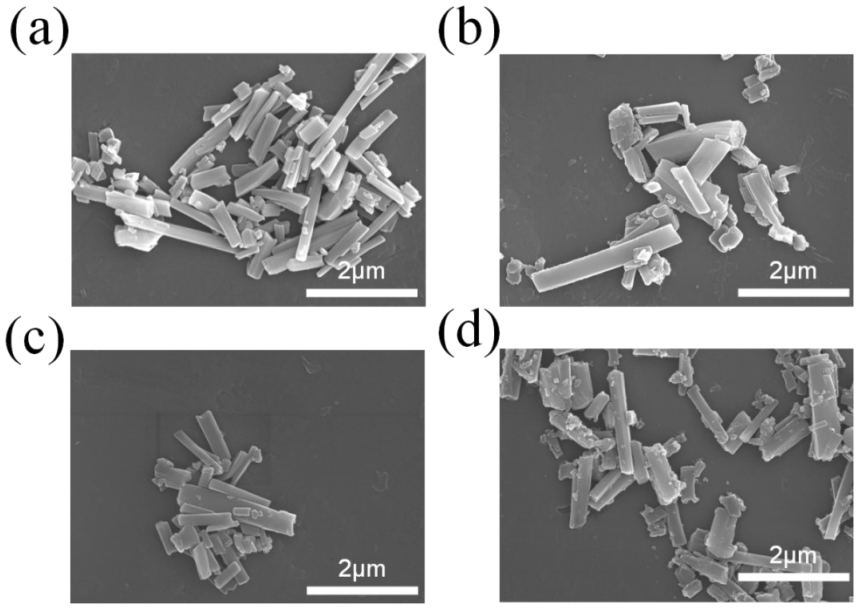

Fig. S1. SEM images of (a) Cu-NDC, (b) Cu/Ni-NDC, (c) Cu/Co-NDC, and (d) Cu/Fe-NDC.

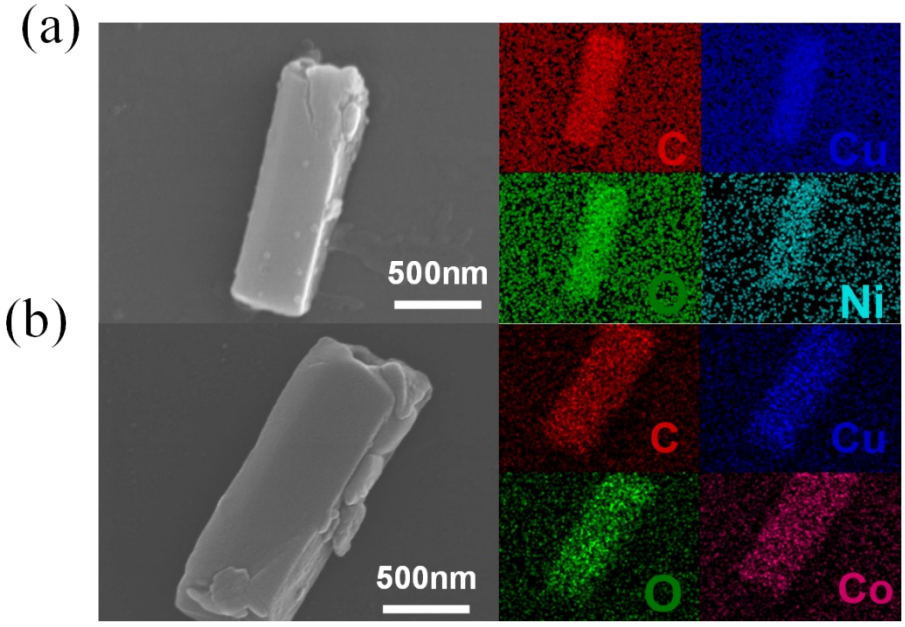

Fig. S2. SEM images and EDS mapping of (a) Cu/Ni-NDC and (b) Cu/Co-N.

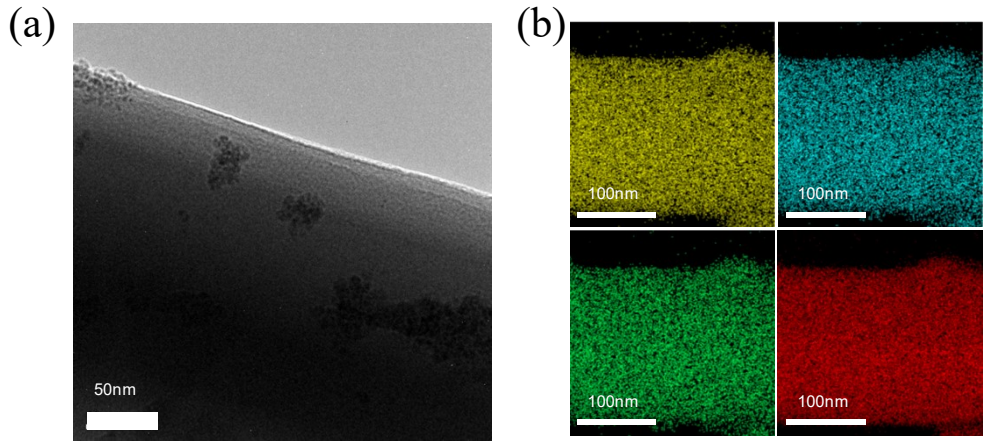

Fig. S3. (a) TEM image and (b) the EDS mapping of Cu/Fe-NDC.

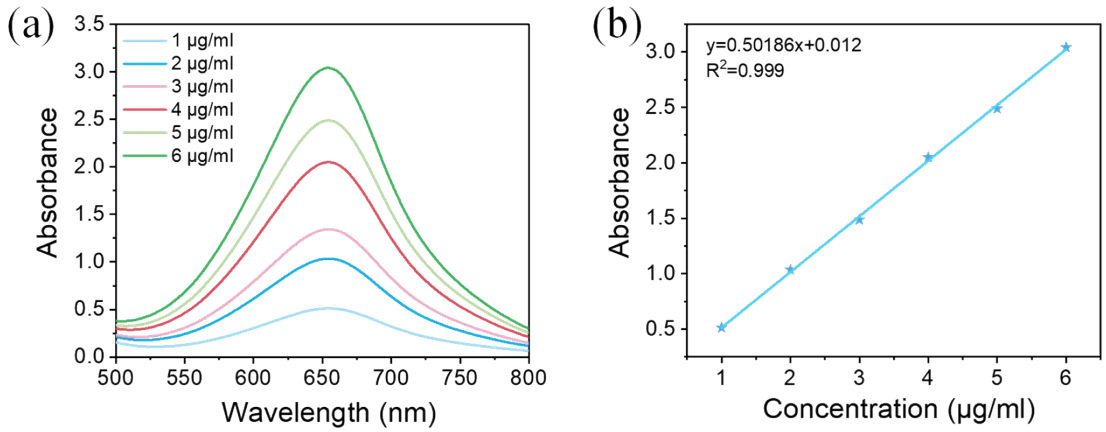

Fig. S4. Calibration of NH_3 concentration using the indophenol blue method: (a) UV-vis spectra and (b) corresponding calibration curve.

A series of NH_4Cl standard solutions (1, 2, 3, 4, 5 and 6 μg/mL) were prepared by diluting a 100 μg/mL stock solution to establish the calibration curve for ammonia determination.

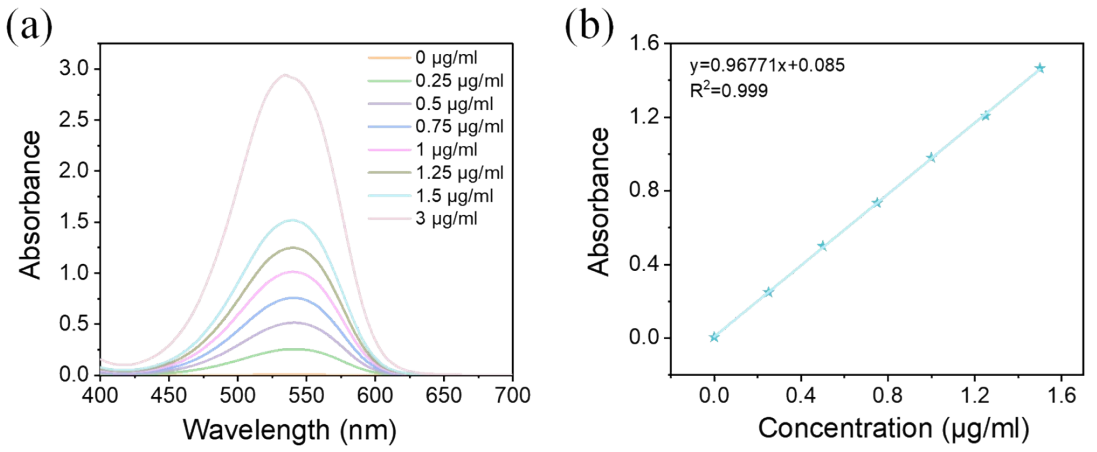

Fig. S5. Calibration of NO_2^- concentration using the indophenol blue method: (a) UV-vis spectra and (b) corresponding calibration curve.

Standard nitrite solutions (0.0, 0.25, 0.5, 75, 1.0, 1.25, 1.5, and 3 μg/mL) were prepared via serial dilution of a 100 μg/mL $NaNO_2$ stock solution to establish the calibration for nitrite quantification.

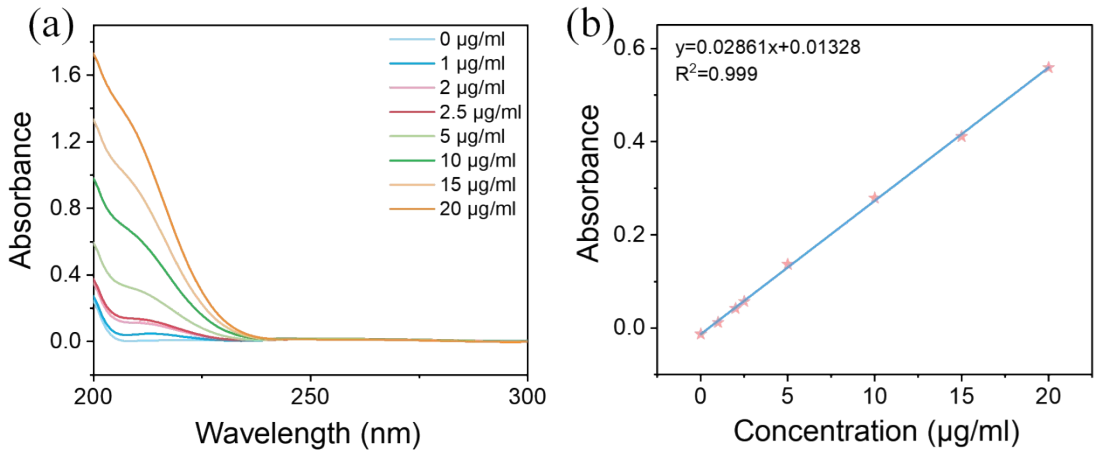

Fig. S6. Calibration of NO_3^- concentration using the indophenol blue method: (a) UV-vis spectra and (b) corresponding calibration curve.

Standard nitrate solutions (0.0, 1.0, 2.0, 2.5, 5.0, 10.0, 15.0, and 20.0 μg/mL) were derived from a 100 μg/mL KNO_3 stock solution via serial dilution to establish the calibration for nitrate quantification.

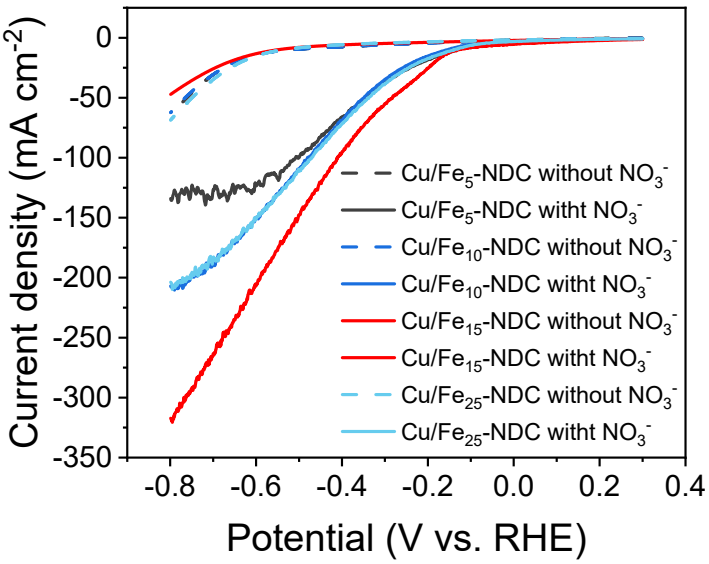

Fig. S7. LSV curves of Cu/Fe_x-NDC with different Cu/Fe molar ratios in 1 M KOH with and without 0.1 M KNO_3.

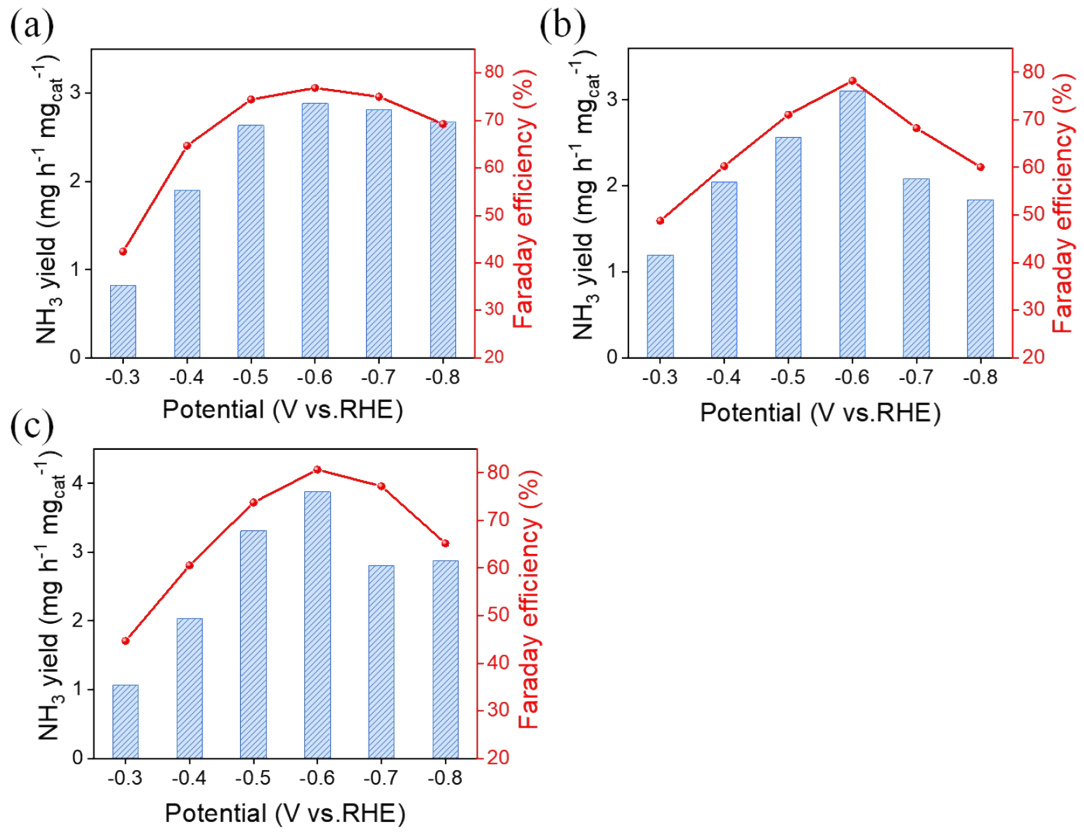

Fig. S8. Potential-dependent NH_3 yield and FE for (a) Cu-NDC, (b) Cu/Ni-NDC, and (c) Cu/Co-NDC.

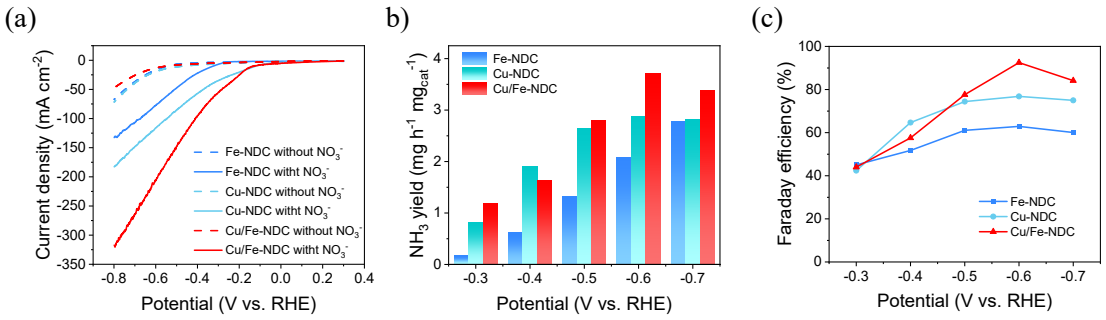

Fig. S9. Electrocatalytic NO_3RR performance comparison of Fe-NDC, Cu-NDC, and Cu/Fe-NDC. (a) LSV curves in 1 M KOH with and without 0.1 M KNO_3. (b) NH_3 yields and (c) Faradaic efficiencies at given potentials.

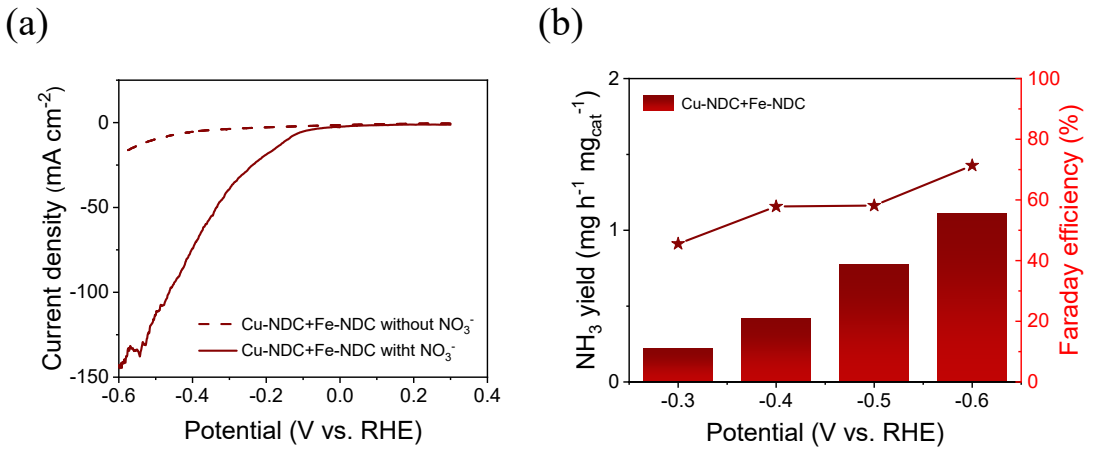

Fig. S10. NO_3RR performance of physically mixed Cu-NDC+Fe-NDC. (a) LSV curves. (b) NH_3 yields and Faradaic efficiencies.

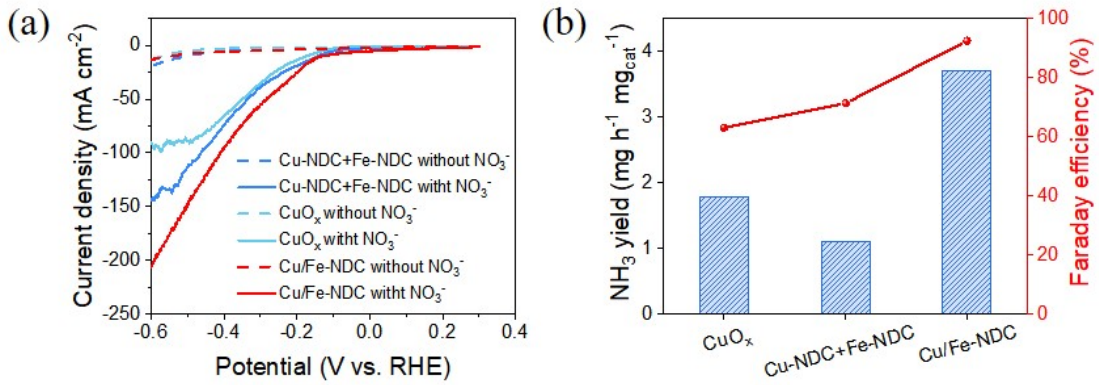

Fig. S11. Electrocatalytic NO3RR performance comparison. (a) LSV curves of the physically mixed Cu-NDC+Fe-NDC, the benchmark CuO_x, and Cu/Fe-NDC in 1 M KOH with and without 0.1 M KNO_3. (b) Corresponding NH_3 yields and Faradaic efficiencies at the optimal potential.

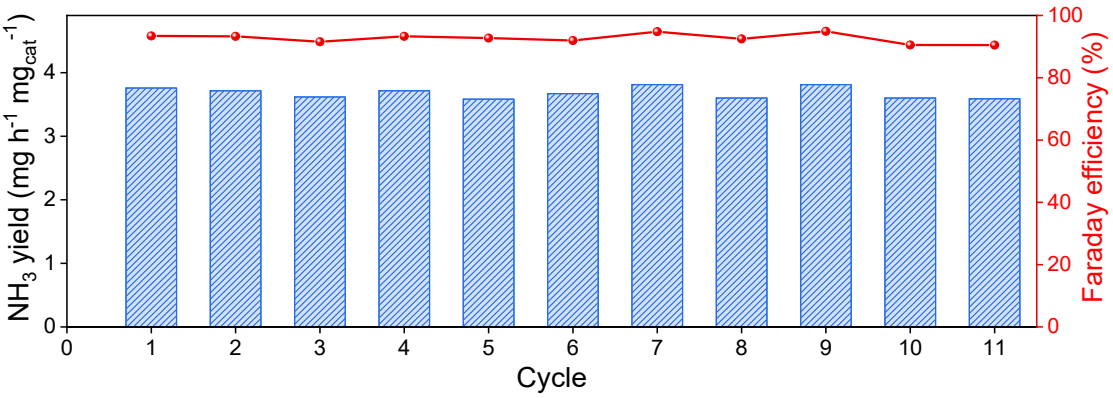

Fig. S12. Long-term electrocatalytic cycling stability of Cu/Fe-NDC for 11 cycles.

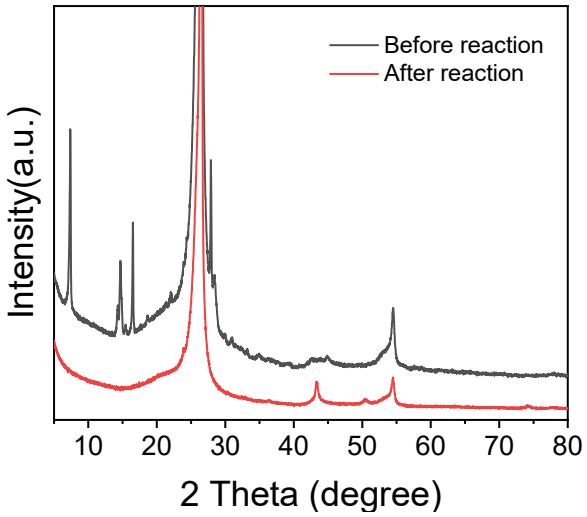

Fig. S13. XRD patterns of the Cu/Fe-NDC deposited on a carbon paper substrate before and after the NO_3RR electrocatalytic test.

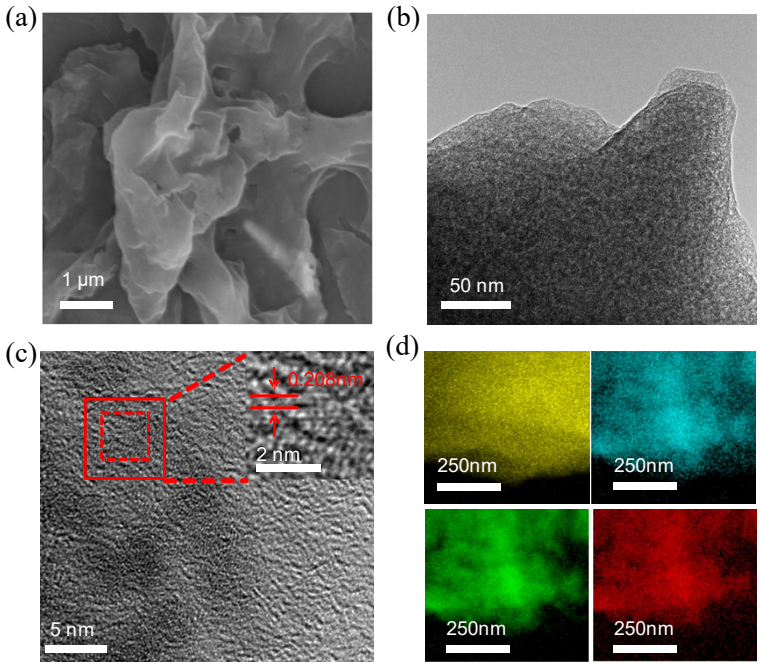

Fig. S14. Morphological and structural characterizations of the post-reaction Cu/Fe-NDC catalyst. (a) SEM, (b) TEM, and (c) HRTEM images. (d) EDS elemental mapping.

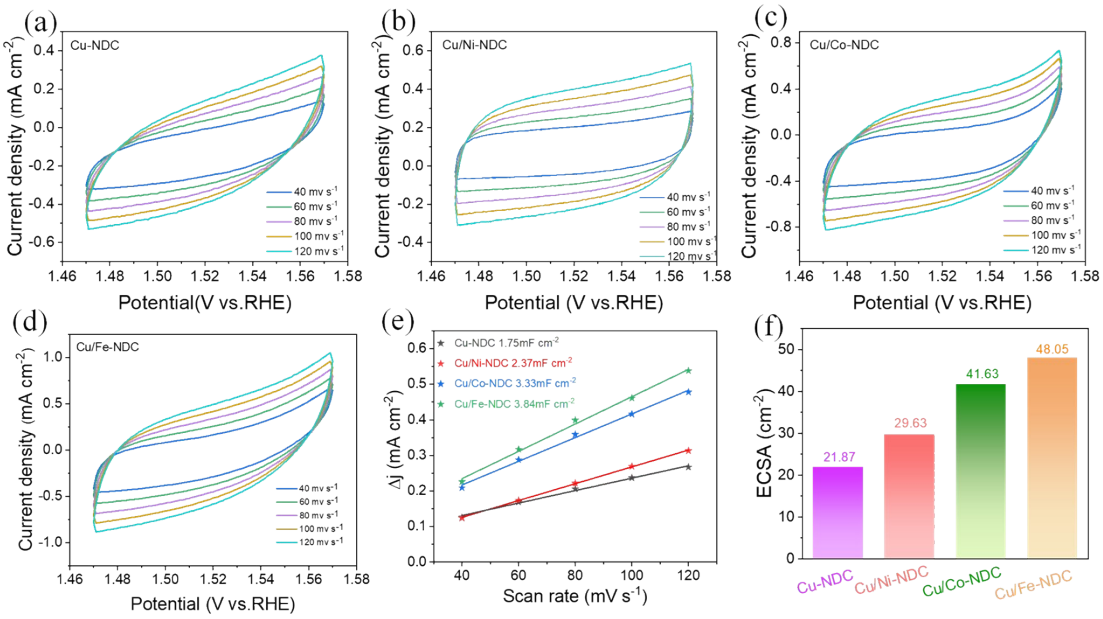

Fig. S15. ECSA evaluation: (a–d) CV curves at various scan rates and (e) linear fitting of current density; (f) calculated ECSA values.The determined ECSA values based on the equation of ECSA = Cdl/Cs × A, where Cdl is the double−layer capacitance of catalyst, Cs is the capacitance of an atomically smooth planar surface (0.04 mF cm^{-2} in alkaline Media), and A is the electrode geometric area.

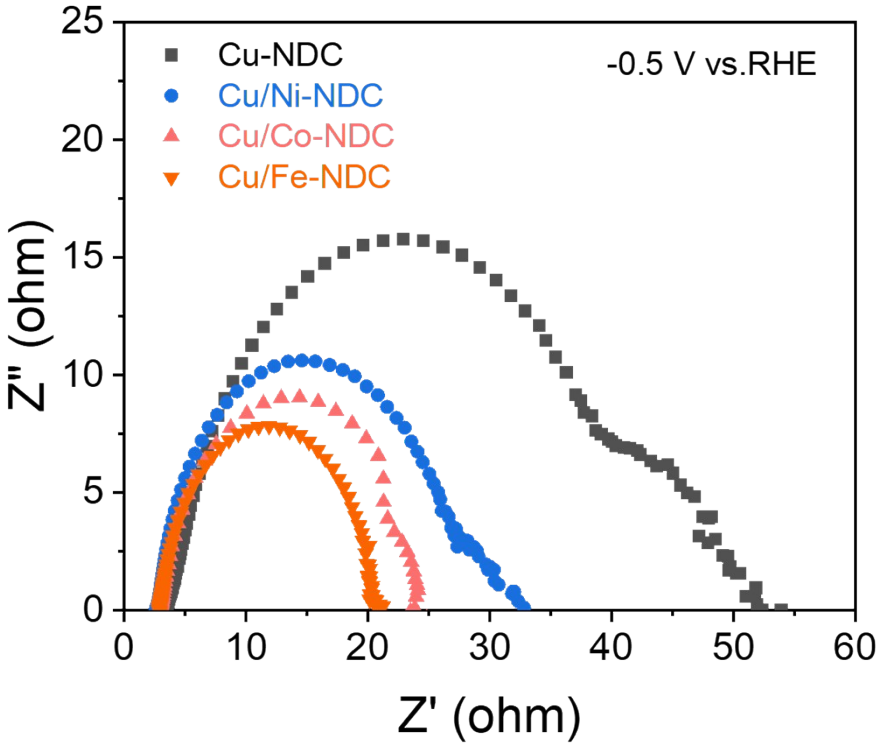

Fig. S16. EIS Nyquist plots of catalysts at −0.5 V vs. RHE.

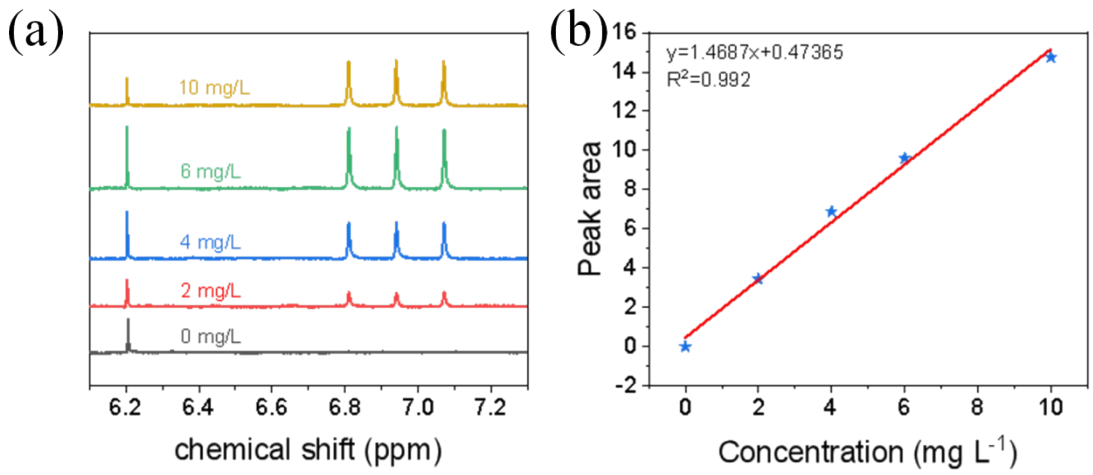

Fig. S17. ^{1}H NMR spectra of electrolyte after ^{+15}N-labeling experiments.

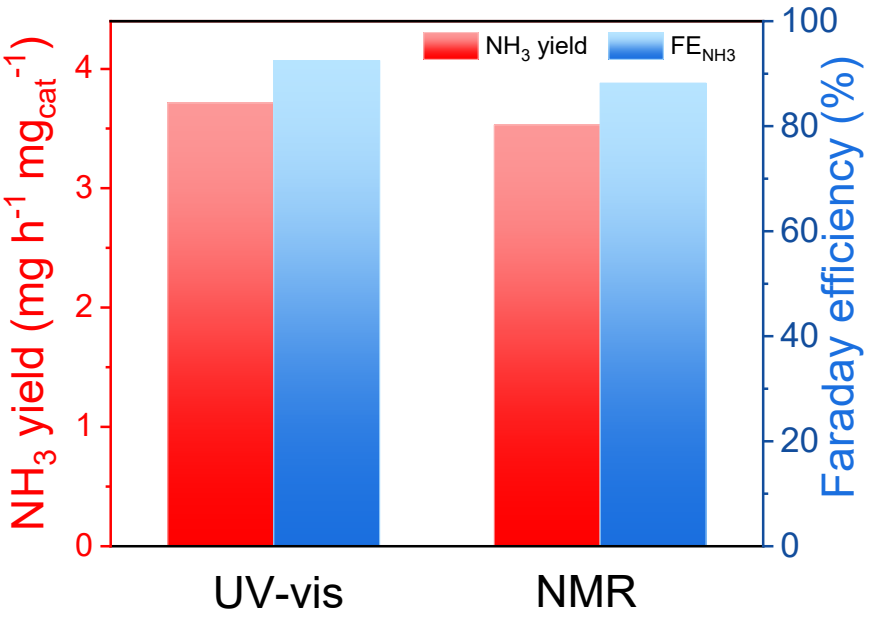

Fig. S18. Correlation between NH_3 yield/FE determined by UV-vis and ^1H NMR methods.

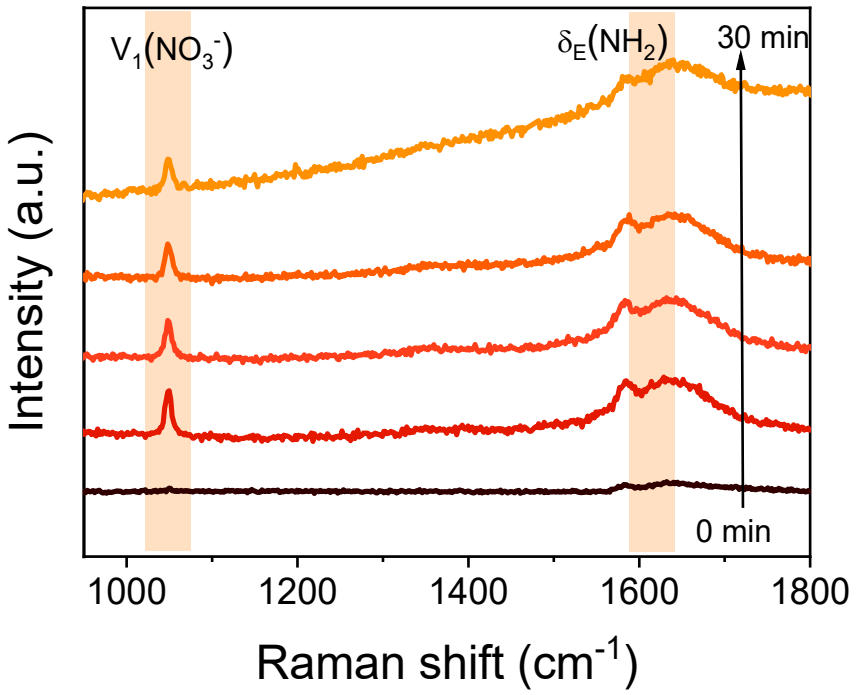

Fig. S19. Time-resolved operando Raman spectra of Cu/Fe-NDC under constant potential.

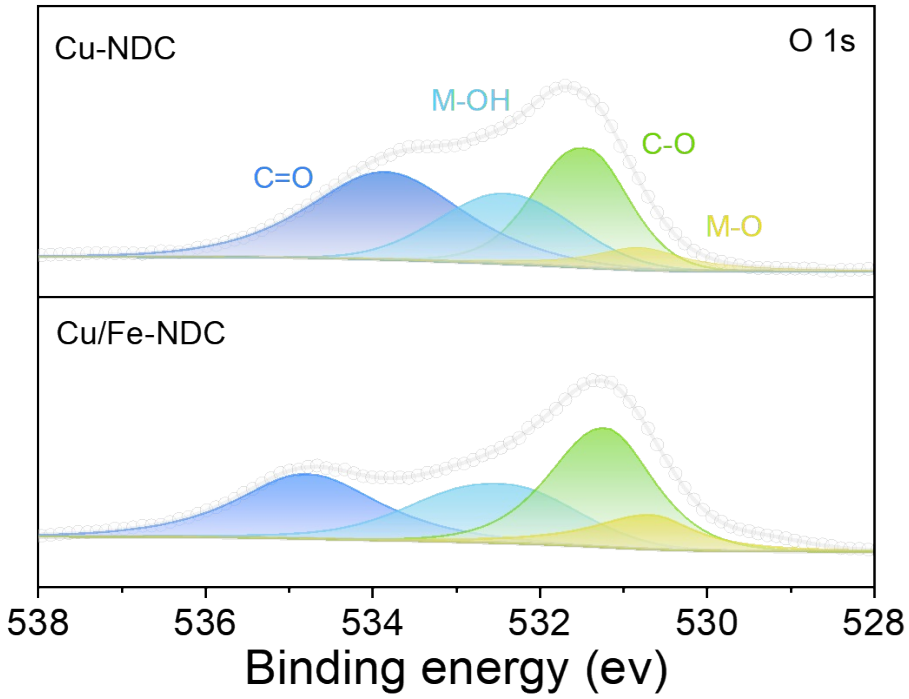

Fig. S20. High-resolution (a) C 1s, (b) O 1s, and (c) Co 2p XPS spectra of Cu/Co-NDC.

Table S1. Elemental composition of samples.

Sample	C(wt%)	O(wt%)	Cu(wt%)	M(wt%)
Cu-NDC	53.88	24.45	21.67	
Cu/Co-NDC	57.95	21.69	17.89	2.5
Cu/Ni-NDC	57.76	24.01	17.11	1.12
Cu/Fe-NDC	49.63	21.81	25.99	2.57

[a]Measured by EDS; [b]measured by ICP-MS.

Table S2. The Zn-NO_3^- battery performance comparison of electrode.

Cathode	OCV (V vs. Zn)	Power density (mW cm^{-2})	Ref.
Cu/Fe-NDC	1.82	12.5	This work
CoSb IMCs/C	1.28	11.88	[1]
15Cu-V_2C MXene	1.52	10.3	[2]
RuFe-NC	1.48	10.16	[3]
0.6W-O-CoP@NF	0.7	9.27	[4]
Cu-RD-KOH	0.939	9.15	[5]
Cu3P@$Co(OH)_2$/CF	0.86	5.16	[6]
Ni-MOF-Ru	1.42	4.99	[7]
HE-OH	1.38	3.62	[8]
Ag/Co_3O_4/CoOOH NMs	1.32	2.56	[9]
NiCoP-VP	1.39	1.1	[10]

Reference

[1]. C. Ma, H. Zhang, J. Xia, X. Zhu, K. Qu, F. Feng, S. Han, C. He, X. Ma, G. Lin, W. Cao, X. Meng, L. Zhu, Y. Yu, A.-L. Wang and Q. Lu, *J. Am. Chem. Soc.*, 2024, **146**, 20069-20079.

[2]. W. Wang, J. Zou, B. Kui, X. Chen, Y. Shen, S. Zhao, G. Zhu, P. Gao and W. Ye, *J. Mater. Chem. A*, 2025, **13**, 35892-35901.

[3]. L. Huang, P. Zhang, X. Ge, B. Wang, J. Yuan, W. Li, J. Zhang, B. Zhang, O. Hanay and L. Wang, *Nano-Micro Lett.*, 2026, **18**, 66.

[4]. Z. Chang, G. Meng, Y. Chen, C. Chen, S. Han, P. Wu, L. Zhu, H. Tian, F. Kong, M. Wang, X. Cui and J. Shi, *Adv. Mater.*, 2023, **35**, 2304508.

[5]. H. Jiang, G.-F. Chen, O. Savateev, J. Xue, L.-X. Ding, Z. Liang, M. Antonietti and H. Wang, *Angew. Chem. Int. Ed.*, 2023, **62**, e202218717.

[6]. H. Jiang, J. Xue, L.-X. Ding, S. Han, G.-F. Chen and H. Wang, *Small Methods*, 2023, **7**, 2300021.

[7]. X. Cai, J. Xu, Y. Yin, G. Qiao, W. Shen, G. Wang and Z. Jiao, *Adv. Funct. Mater.*, 2024, **34**, 2415174.

[8]. M. Chen, X. Li, N. Liu, Z. Du, Z. Wang and J. Qi, *Chin. Chem. Lett.*, 2025, **36**, 111294.

[9]. S. Wu, Y. Jiang, W. Luo, P. Xu, L. Huang, Y. Du, H. Wang, X. Zhou, Y. Ge, J. Qian, H. Nie and Z. Yang, *Adv. Sci*., 2023, **10**, 2303789.

[10]. J. Ye, A. Wang, Y. Yang, X. Qian, C. Wan, G. He and H. Chen, *Chem. Eng. J.*, 2024, **487**, 150434.